Determining effective threshold range of image pixel values for municipal waste contaminated clay

Rui Zhang (05171521@cumt.edu.cn)
China University of Mining and Technology
Liwen Cao
China University of Mining and Technology
Xuehan Feng
Shanghai Municipal Engineering Design Institute Group Co Ltd.Nanjing company
Shenglin Wang
Tongji University
Nian Cai
Fujian College of Water Conservancy and Electric Power
Yuliang Guo
China University of Mining and Technology

Research Article

Keywords: municipal waste, SEM image, threshold, apparent porosity ratio, fractal dimension

Posted Date: March 30th, 2022

DOI: https://doi.org/10.21203/rs.3.rs-1448795/v1

Abstract

Nowadays, more attention has been paid to the study of the properties and structure of contaminated clay, while there are few studies on the microstructure of contaminated clay, especially municipal waste contaminated clay. The purpose of this paper is to determine the threshold range by observing and processing the microscopic images of municipal waste contaminated clay with different seepage depths and concentrations. In this study, contaminated clay samples were taken at different depths in a column test and at different concentrations with $CaCO_3$ and CH_3COOH, imaged through scanning electron microscopy (SEM), and then subjected to binarization. Five steps for determining the pixel thresholds were discussed including: imaging contaminated clay through SEM, preprocessing and binarizing the SEM images with IPP, carrying out morphological processing by using PCAS and determining the pixel threshold value of the SEM images. The apparent porosity ratio of the contaminated clay and the fractal dimension of the clay particles were applied as the parameters for evaluation, the effective threshold range of the image pixel values of the municipal waste contaminated clay was determined to be 110–140. This method is validated by examining the relationship between the pixel threshold value and apparent porosity ratio, the variation in the porosity ratio and apparent porosity ratio with seepage depth, and the different compaction factors with seepage depth.

1. Introduction

Determining effective threshold range of image pixel values for contaminated clay

To evaluating the engineering geological properties of clay, it is of great importance to have a quantitative study of the microstructure of clay (Usov et al., 2018), and pre-processing the SEM images obtained by scanning electron microscopy for quantitative study is a common method for soil microstructure analysis and processing. After enhancement, segmentation, binarization and denoising of SEM images, black and white pixels in black and white images represent the pores and particles of clay, respectively. This is because different pixel threshold values generate different grayscale levels and textures. The porosity obtained from the SEM image processing is affected by the selected threshold greatly (Wang et al., 2004). The grayscale threshold values of intensity are 0 (pure white) ~ 255 (pure black). Therefore, different microstructural parameters are obtained for the same type of clay with the same research method through different pixel threshold values. The pixel threshold value thus has great significance for studies on the clay microstructure.

To date, a good number of threshold algorithms have been developed, such as Otsu's (Barros Wysterlânya K P et al., 2021; S. Song et al., 2021), iteration (Han Ningning et al.;Drever et al., 2007; Goh et al., 2018), image histogram (Zhenghua Huang et al., 2021), entropy criterion (Wang Gang et al, 2021), Grey Wolf Optimizer (GWO) (Hatta,N.M. et al, 2019), edge detection (Huizhi Chi and Yu Tian,2021), clustering (Singla and Patra, 2017;Mittal,H. et al,2021), Whale Optimization (WOA) (Aziz et al., 2017;Mirjalili,S and Lewis,A, 2016; Kaveh and Ghazaan, 2017), Moth-Flame Optimization (MFO) (Aziz et al., 2017;Shehab,M. et al,2020), and hybrid method (Patra,S. et al, 2011). Each algorithm has its own characteristics. For

example, Otsu's algorithm uses the largest interclass variance to find the optimal threshold, and its computational complexity increases exponentially with more thresholds (Khairuzzaman and Chaudhury, 2017). An algorithm based on image histograms has the advantages of small storage space, high processing speed, and ease of operation (Patra et al., 2011). The WOA does not need structural adjustments to solve different optimization problems because this algorithm only has two main parameters to be adapted (Farhad,S.G. and Hojjat,G., 2019). The study of the nature and structure of contaminated soil is gradually gaining attention, and the structure and threshold values of contaminated soil have an important influence on the prediction of its engineering properties, while the study of microstructure of contaminated soil from municipal waste, especially the judgment of threshold values, is equally important.

In this paper, the microscopic structure of municipal waste contaminated clay was taken as the research object. Images of the contaminated clay samples were taken with a scanning electron microscope and then analyzed by Image-Pro Plus image analysis software as well as PCAS (Pores (Particles) and Cracks Analysis System) software. Variations in the microstructure of the contaminated clay with different percolation depths of municipal waste contaminants, i.e., different levels of contamination and different concentrations of $CaCO_3$ and CH_3COOH in the late stage of degradation of municipal waste contaminants were found and the effective threshold range of image pixel values was determined. The study findings are expected to serve as guidelines for threshold value, extraction of microstructure parameters of contaminated clay and evaluation of engineering geological properties of contaminated soil.

2. Experimental

2.1 Testing equipment and procedures

This study was designed to prepare two types of contaminated clay from municipal waste, one obtained by the seepage of municipal waste pollutants (mainly leachate) and the other by soaking the products of the degradation of municipal waste pollutants in the later stage, i.e., the seepage municipal waste contaminated soil and the soaking municipal waste contaminated soil.

The seepage municipal waste contaminated soil toke clay with different seepage depths of source pollution as the research object, and the soaking municipal waste contaminated soil toke the contaminated clay prepared by $CaCO_3$ and CH_3COOH in the post-degradation stage of municipal waste pollutants was taken as the research object. The clay used in the experiment in this study originated from the suburbs of the south region of Xuzhou City in Jiangsu Province, China, after impurity removal, air drying and screening. The basic physical properties of clay are shown in Table 1.

Table 1
physical properties of clay

Sample	Density(ρ)g/cm^3	Specific gravity (Gs)	Water content(w) %	Dry density(ρ_s) g/cm3	Void ratio (e_0)	Liquid limit(w_L) %	Plastic limit(w_P) %
Clay	1.735	2.740	21	1.434	0.9722	40.5	21.3

When the municipal waste contaminated clay with different seepage depths was prepared, the clay was compacted layer by layer into the test device, and the height of the clay column was about 100 cm. A gravel drainage layer was placed on top of the compacted clay layer. Following that, municipal domestic waste was graded and compacted, and a layer was placed above the gravel drainage layer. The experimental setup was based on the liner system of a domestic waste landfill in Xuzhou City, which uses compacted clay. This liner system was used to design the column for testing the municipal waste contaminated clay (see schematic in Fig. 1). Municipal waste pollutants (leachate) seeped through the clay layer by pressure pump at a rate of 38.5L/d and the seepage level in the column was maintained at 1 m above the clay layer. And the water quality of municipal waste pollutants (leachate) is shown in Table 2. Six sampling holes were drilled into the column at depths of 3.1 cm, 17.3 cm, 36.8 cm, 48.5 cm, 56.3 cm, and 75.8 cm from the surface of the compacted clay layer.

Table 2
Water quality of leachate in simulating landfill experiment

Parameters		Parameters		Parameters	
COD (mg/L)	19500	Mg (u/g)	414	Mn (u/g)	0.3734
BOD (mg/L)	9833	K (u/g)	1639	Pb (u/g)	0.0289
TSS (mg/L)	1334.59	Na (u/g)	3319	Cu (u/g)	0.0253
VSS (mg/L)	576.89	As (u/g)	0.0855	Si (u/g)	8.7
NH_4^+-N (mg/L)	1701.8	B (u/g)	3.88	Al (u/g)	2.3
Ca (u/g)	186	Cd (u/g)	0.0005	Total hardness (mg/L)	1746.455
pH	6.57	Hg (u/g)	0.0049	Total alkalinity (mg/L)	12410.09
TVFA (mmol/L)	63	Ni (u/g)	0.2306		
Fe (u/g)	20	Zn (u/g)	0.6148		

In order to study the threshold problem of municipal waste contaminated clay from another point of view, the contaminated clay in the later stage of degradation of municipal waste pollution was selected. Since the municipal waste pollutant mass is continuously degraded during the process of seepage and the main products of late degradation are $CaCO_3$ and CH_3COOH, $CaCO_3$ and CH_3COOH polluted clay with

concentrations of 0.2mol/L, 0.4mol/L, and 0.6mol/L were manually configured by soaking the clay as the soaking municipal waste contaminated soil.

2.2 Sample preparation and properties

The seepage municipal waste contaminated soil was obtained by extracting six sets of contaminated clay samples with different seepage depths from six sampling holes of the seepage municipal waste contaminated soil preparation test device, that is, on behalf of the municipal waste pollution quality of different degrees of pollution of soil samples, while uncontaminated clay samples were also prepared as the control. Different seepage depth soil properties are shown in Table 3. The soaking municipal waste contaminated soil was obtained by six groups of $CaCO_3$ and CH_3COOH contaminated soil samples with concentrations of 0.2mol/L, 0.4mol/L and 0.6mol/L. The samples that would undergo SEM were prepared in accordance with the specifications of the scanning electron microscope with as little disturbance as possible. The clay was cut and trimmed into samples with dimensions of 1cm×1cm×1cm. The samples were then dried at a low-temperature in an oven. After the samples were air dried, loose particles on the cross-section of the clay were removed with tape until the clay surface was smooth with no loose particles.

Table 3
Physical parameters of contaminated clay samples at different depths of column after seepage

Depth of sampling hole (cm)	**3.1**	**17.3**	**36.8**	**48.5**	**56.3**	**75.8**
Dry density (g/cm$^{3)}$	1.55	1.55	1.5	1.53	1.53	1.56
Porosity ratio	0.34	0.64	0.73	0.79	0.81	0.83
Saturated water content (%)	28.38	29.12	28.42	28.02	27.78	26.52
Organic silt produced per kg of clay (%)	13.85	12.37	8.81	7.12	6.33	4.61
Calcium carbonate produced per kg of clay (g)	5.68	4.98	4.49	4.38	3.78	2.24

3. Determining Effective Threshold Range Of Image Pixel Values For Contaminated Clay

3.1 Image processing method: Image-Pro Plus and PCAS

Image-Pro Plus converts a color image into a grayscale image and then converts the grayscale image into a binary image. This software can extract more than 60 measured parameters by measuring the attributes of objects, including area and perimeter, measuring the lengths of lines and short axis, focusing on the center point of a z-stack, as well as reporting on the fractal dimension of an object, etc. These could be done both manually and automatically. The measured parameters are selected based on the requirements of the user. The target parameters are then shown and the targets automatically numbered. The main

function of PCAS is to identification, geometric quantification and statistical analysis of microscopic images of particles, cracks and pores. PCAS can automatically remove noise from binary images, automatically segment and accurately identify soil pores (Chun L. et al,2011). SEM image processing steps are shown in Fig. 2.

(1) Pre-processing of SEM Images

The SEM image of undisturbed soil was selected as an example to illustrate the SEM image preprocessing method. First, Image-Pro Plus was used to correct distortions of the image background, and eliminate uneven brightness. Then, the background corrected image was processed to enhance the contrast of image intensity by adjusting the brightness, contrast and gamma correction. Finally, filter was used to improve the measurement accuracy and image quality.

(2) Thresholding of SEM Images

In carrying out the image segmentation of processed images in Image-Pro Plus, the range limit bar was dragged into the image segmentation dialog box to change the threshold pixel value to a value that is between 0 to 255 and the original image was continuously compared to the image with changing pixel values. Visual segmentation was adopted and carried out multiple times to reduce errors until there was optimal segmentation.

(3) Morphological Processing of SEM Images

After binarizing the threshold image, some isolated black spots and bright spots were found, and this study dealt with the isolated spots with the help of automatic analysis of the pore system of PCAS. Through the corrosion operation on the image, the fine connections between pores were eliminated, so as to identify and separate the particles that contact and overlap each other in the image. Image-Pro Plus was also used to quickly obtain parameters such as the diameter, area, perimeter, fractal dimension, and roundness of the contaminated clay particles and pores.

3.2 Morphology of Microstructure of Contaminated Clay

The control sample and seepage municipal waste contaminated soil samples (taken at column depths of 3.1 cm, 17.3 cm, 36.8 cm, 48.5 cm, 56.3 cm and 75.8 cm) and uncontaminated soil and soaking municipal waste contaminated soil samples (concentration were 0.2mol/L, 0.4mol/L, 0.6mol/L $CaCO_3$ and CH_3COOH) were scanned at different magnifications (1200, 1500, 1800, and 2100 x). The research results of Tang et al. (2008) were incorporated, it is not the case that the larger the magnification is, the better the observation effect is, and the magnification is selected in the range of 1500 ± 300 as the best. Therefore, SEM images magnified 1500 x were selected for the control sample and seepage municipal waste contaminated soil samples, and SEM images magnified 1200 x were selected for uncontaminated soil and soaking municipal waste contaminated soil samples. Before the observation, the sample table was cleaned by the cleaning instrument, and then a small amount of conductive adhesive was dipped with a wooden stick, and the sample was firmly plated with gold on the clay surface. The SEM images of

the control sample and seepage municipal waste contaminated soil samples at depths of 17.3 cm, 56.3 cm and 75.8 cm and the binary images after treatment are shown in Fig. 3. The SEM images of uncontaminated soil and $CaCO_3$ and CH_3COOH contaminated soil samples at concentration of 0.2 mol/L, 0.4mol/L and 0.6mol/L and the binary images after treatment are shown in Fig. 4.

3.3 Effective threshold range of image pixel values based on apparent porosity ratio of contaminated clay

The pore size, pore area and fractal dimensions were used as the measured parameters of the pores, and particle size, area and quantity, fractal dimension of the particles, and other parameters were applied as the measured parameters of the clay particles. Using the data collected by Image-Pro Plus, the apparent porosity ratios and image pixel values for the seepage municipal waste contaminated soil are plotted in Fig. 5, the apparent porosity ratios and image pixel values for the soaking municipal waste contaminated soil are plotted in Fig. 6.

Table 1 shows that the porosity ratio of the whole soaking municipal waste contaminated soils is 0.97. Table 3 shows that the porosity ratio of the seepage municipal waste contaminated clay at column depths of 3.1 cm, 17.3 cm, 36.8 cm, 48.5 cm, 56.3 cm, and 75.8 cm is 0.34, 0.64, 0.73, 0.79, 0.81, and 0.83, respectively. At a pixel value of 130, the apparent porosity ratio of the clay at a column depth of 3.1 cm is about 0.31 which approximates the measured porosity ratio of 0.34. Therefore, a pixel value of 130 is recommended for the clay sample at a column depth of 3.1 cm. Similarly, the pixel value for the clay samples based on the proximity of the apparent porosity ratio to the measured porosity ratio at column depths of 17.3 cm, 36.8 cm, 48.5 cm, 56.3 cm, and 75.8 cm is 130, 130, 130, 110, and 110, respectively. The reasonable pixel value of $CaCO_3$ contaminated clay with concentrations of 0.2mol/L, 0.4mol/L and 0.6mol/L is 120, 130 and 140, respectively. The reasonable pixel value of CH_3COOH contaminated clay with concentrations of 0.2mol/L, 0.4mol/L and 0.6mol/L is 130, 130 and 110, respectively.

3.4 Effective threshold range of image pixel values based on fractal dimension of contaminated clay particles

Fractal theory uses fractal dimension to describe the shape of particles (Pi,Z. et al., 2021). The fractal dimension is determined by image analysis to quantify the soil structure (Nakatsuka et al., 2016). Many previous studies have shown that fractal dimension is a commonly used parameter to study the microstructure of soil (Hong Sun et al., 2020; Risović, D. et al., 2008; Zou X. et al, 2021; Munoz et al., 2014).

The relationship between fractal dimension and the image pixel threshold value of the seepage municipal waste contaminated soil and the soaking municipal waste contaminated soil is plotted in Fig. 7 and Fig. 8.

With increases in the pixel value, the fractal dimension of the particles increases at first, then tends to a constant value, and then decreases substantially. Tang et al. (2008) indicated that the fractal dimension

of clay particles should be examined within the constant interval. The fractal dimension of the contaminated clay particles at a column depth of 3.1 cm has a relatively constant value at a pixel value interval of 110 ~ 170. Similarly, the pixel value interval for the fractal dimension of the seepage municipal waste contaminated clay particles at a column depth of 17.3 cm, 36.8 cm, 48.5 cm, 56.3 cm and 75.8 cm is 110 ~ 190, 110 ~ 190, 110 ~ 210, 110 ~ 170, and 90 ~ 150, respectively; the pixel value interval for the fractal dimension of $CaCO_3$ contaminated clay with concentrations of 0.2mol/L, 0.4mol/L and 0.6mol/L is 80 ~ 150, 110 ~ 140 and 90 ~ 180, respectively; the pixel value interval for the fractal dimension of CH_3COOH contaminated clay with concentrations of 0.2mol/L, 0.4mol/L and 0.6mol/L is 100 ~ 140,110 ~ 150 and 100 ~ 180, respectively. In summary, the optimal pixel value interval is between 110 and 140 based on the morphological structure of the contaminated clay particles, and calculations based on this range are more reliable.

3.5 Determining effective threshold range of image pixel values for contaminated clay

The focus is on the clay pores and particles when the clay microstructure is examined. The optimal threshold range of image pixel values needs to take the pores and particles of clay into consideration. In this study, the effective threshold range of image pixel value was found to be 110–140. When the fractal dimension of the contaminated clay particles was also taken into consideration, the effective threshold range of the pixel value was 110–140. Therefore, the optimal threshold range of the pixel value based on the microscopic structure of municipal waste contaminated clay was 110–140.

4. Validation And Discussion Of Validity Of Threshold Range Of Image Pixel Values

Figure 9 shows the binarization of the SEM images of CH_3COOH contaminated clay with concentration of 0.6mol/L for 12 different image pixel values (T denotes the pixel value). Three image pixel values near the effective threshold range, 70, 110, and 180 were selected and plotted (see in Fig. 10). The effective threshold range of 110–140 is validated based on the following three factors.

First, there is the relationship between the effective threshold range of image pixel values and the apparent porosity ratio. The same SEM images of municipal waste contaminated clay resulted in different threshold ranges of image pixel values, which result in different binary images. A larger threshold range of image pixels means that more pixels are considered to be the pores, that is, the number of black pixels increases, and the apparent porosity ratio increases. Figure 9 shows this phenomenon. At the same time, when the pixel threshold value is 130, the porosity ratio most approximates the actual porosity ratio.

Second, there are the variations in pore blockage with depth of seepage. Greater depth of seepage of municipal waste pollutants means reduced likelihood of clay contamination, and higher apparent porosity ratio and porosity ratio. The reason is because when waste pollutants seep, organic matter (organisms) and suspended matter block the pores, and organic matter and its degradation object chemically react

with the clay to form calcium carbonate and other deposits in the clay pores. The amount of organic matter per kilogram of clay produced and the amount of calcium carbonate per kilogram of clay produced are shown in Fig. 10. The two slopes demonstrate this rationale, thus indicating that the method in this study is reasonably accurate.

Third, the rationality of the effective threshold range from the perspective of macroscopic parameters is determined. In this study, the parameter that reflects the effective combination of macroscopic properties (dry density) and microstructure (apparent porosity ratio) of the clay was defined as the compaction factor. The compaction factor was equal to the ratio of the dry density to the apparent porosity ratio. The compaction factor is plotted with seepage depth and concentration of contaminations with pixel values of 70, 110, and 180, as shown in Fig. 11 and Fig. 12, respectively. It can be seen from Figs. 11 and 12 that selections of the pixel values have a significant impact on the compaction factor. At the same seepage depth or the same contaminant concentration, a larger pixel threshold value results in a smaller compaction factor, which is consistent with the relationship between clay compactness and pore size. When the pixel threshold value is 180, the compaction factor for each depth of seepage is small, and when the pixel threshold value is 70, the compaction factor is large, which is not in agreement with the actual clay. In addition, it can be seen from Fig. 11 that under different pixel threshold values, the compaction factor is reduced with increased depth of the seepage, and the compactness of the clay is also reduced, which is in agreement with the conclusion that the porosity ratio of municipal waste contaminated clay increases with seepage of pollutants. It can be seen from Fig. 12 that under different pixel threshold values, the compaction factor increases with the increase of $CaCO_3$ concentration, and decreases with the increase of CH_3COOH concentration, which is consistent with the conclusion that $CaCO_3$ plays a cementation effect on soil and CH_3COOH plays a corrosion effect on soil. Therefore, it is reasonable to conclude that the pixel threshold value ranges from 110 to 140.

5. Conclusions

(1) For numbered lists The threshold was determined by binarization and morphological processing of SEM images using IPP and PACS. Image Pro Plus is used to preprocess and binarize SEM images to eliminate uneven brightness. The particles that come into contact and overlap each other are identified and separated in the image by using PACS. Through the combination of IPP and PACS image processing method, the pixel threshold value was more accurate.

(2) The dry density, porosity ratio, organic silt content found in the pores, and water content were applied based on the relationship between the pixel threshold value and apparent porosity ratio, as well as the relationship between the pixel threshold value and fractal dimension of clay particles. The range of the pixel threshold value of municipal waste contaminated clay was concluded to be 110–140.

(3) The pixel threshold value range of 110–140 of municipal waste contaminated clay was validated based on the relationship between the pixel threshold value and apparent porosity ratio, the variations in

pore blockage with depth of seepage, and the different compaction factors with seepage depth and contaminant concentrations.

Declarations

Acknowledgements: This study is supported by the National Natural Science Foundation of China (No. 41972281, 41727801, 41372326). A Project Funded by the Priority Academic Program Development of Jiangsu Higher Education Institutions.

Competing Interests：No conflict of interest exits in the submission of this manuscript, and manuscript is approved by all authors for publication. I would like to declare on behalf of my co-authors that the work described was original research that has not been published previously, and not under consideration for publication elsewhere, in whole or in part. All the authors listed have approved the manuscript that is enclosed.

Author Contributions：All authors contributed to the study conception and design. Material preparation, data collection and analysis were performed by Liwen Cao, Xuehan Feng, Shenglin Wang, Nian Cai and Yuliang Guo. The first draft of the manuscript was written by Rui Zhang and all authors commented on previous versions of the manuscript. All authors read and approved the final manuscript.

References

1. Aziz MAE, Eweesc AA, Hassanien AE (2017) Whale Optimization Algorithm and Moth-Flame Optimization for multilevel thresholding image segmentation. Expert Syst Appl 83:242–256
2. Barros Wysterlânya KP, Dias Leonardo A, Fernandes Marcelo AC (2021) Fully Parallel Implementation of Otsu Automatic Image Thresholding Algorithm on FPGA.[J].Sensors (Basel, Switzerland), 21(12)
3. Tang C, Shi B, Wang B Factors affecting analysis of soil microstructure using SEM [J].Chinese Journal of Geotechnical Engineering, 2008(04):560–565.(Chinese)
4. Chun Liu B, Shi J, Zhou (2011) Chaosheng Tang,Quantification and characterization of microporosity by image processing, geometric measurement and statistical methods: Application on SEM images of clay materials. Appl Clay Sci Volume 54(1):97–106
5. Drever L, Roa W, McEwan A, Robinson D (2007) Iterative threshold segmentation for PET target volume delineation. Med Phys 34(4):1253–1265
6. Farhad Soleimanian Gharehchopogh and Hojjat Gholizadeh (2019) A comprehensive survey: Whale Optimization Algorithm and its applications[J]. Swarm Evol Comput 48:1–24
7. Goh TY, Basah SN, Yazid H, Safar MJA, Saad FSA (2018) Performance analysis of image thresholding: Otsu technique. Measurement 114:298–307
8. Han Ningning and Li Shidong and Song Zhanjie (2021) Efficient iterative thresholding algorithms with functional feedbacks and null space tuning[J].Signal Processing,188

9. Hatta NM, Zain AM, Sallehuddin R et al (2019) Recent studies on optimisation method of Grey Wolf Optimiser (GWO): a review (2014–2017). Artif Intell Rev 52:2651–2683
10. Hong S et al (2020) Microstructure investigation of soft clay subjected to triaxial loading[J].Engineering Geology,274
11. Chi H, Tian Yu Analysis and Research of Image Edge Detection Algorithms. [J].Electronic Product Reliabilty and Enviromental Testing,2021, 39(04):92–97.(Chinese)
12. Khairuzzaman AKM, Chaudhury S (2017) Multilevel thresholding using grey wolf optimizer for image segmentation. Expert Syst Appl 86:64–76
13. Mirjalili S, Lewis A (2016) The Whale Optimization Algorithm. Adv Eng Softw 95:51–67
14. Mittal H, Pandey AC, Saraswat M et al (2021) A comprehensive survey of image segmentation: clustering methods, performance parameters, and benchmark datasets.Multimed Tools Appl
15. Munoz FJ, Martinez FSJ, Caniego FJ (2014) Fractal parameters of pore space from CT images of soils under contrasting management practices. Fractals-Complex Geom Patterns Scaling Nat Soc 22(3):9
16. Nakatsuka H, Oda M, Hayashi Y, Tamura K (2016) Effects of fresh spent mushroom substrate of Pleurotus ostreatus on soil micromorphology in Brazil. Geoderma 269:54–60
17. Patra S, Ghosh S, Ghosh A (2011) Histogram thresholding for unsupervised change detection of remote sensing images. Int J Remote Sens 32(21):6071–6089
18. Pi Z, Zhou Z, Li X, Wang S (2021) Digital Image Processing Method for Characterization of Fractures, Fragments, and Particles of Soil/Rock-Like Materials. Mathematics 9:815
19. Risović D, Mahović,Furić S et al (2008) Inferring fractal dimension of rough/porous surfaces—A comparison of SEM image analysis and electrochemical impedance spectroscopy methods.[J]. Appl Surf Sci 255(5):3063–3070
20. Shehab M, Abualigah L, Hamad A (2020) Moth–flame optimization algorithm: variants and applications. Neural Comput & Applic 32:9859–9884
21. Singla A, Patra S (2017) A fast automatic optimal threshold selection technique for image segmentation. Signal Image and Video Processing 11(2):243–250
22. Song S, Gao T (2021) "Research on image segmentation algorithm based on threshold," 2021 13th International Conference on Measuring Technology and Mechatronics Automation (ICMTMA), pp. 306–308, doi: 10.1109/ICMTMA52658.2021.00071
23. Usov AN, Chernov MS, Sokolov VN, Voznesensky EA (2018) Variation in the Microstructure of Clay Soil during Deformation under Triaxial Compression with Consideration of the Occurrence of Deformation Instability. Mosc Univ Geol Bull 73(1):83–86
24. Wang B, Shi B, Liu Z, Cai Y (2004) Fractal study on microstructure of clayey soil by GIS. Chin J Geotech Eng 26(2):244–247 (in Chinese)
25. Wang, Gang et al (2021) Adaptive filtering based on recursive minimum error entropy criterion[J]. Sig Process 179:107836

26. Zhenghua Huang Z, Wang J, Zhang Q, Li Yu Shi.Image enhancement with the preservation of brightness and structures by employing contrast limited dynamic quadrihistogram equalization,Optik,Volume 226, Part 1,2021,165877.
27. Zou X, Zhang Z, Wu M, Wan Y (2021) Slope-scale spatial variability of fractal dimension of soil particle size distribution at multiple depths. Soil Sci Soc Am J 85:117–131

Figures

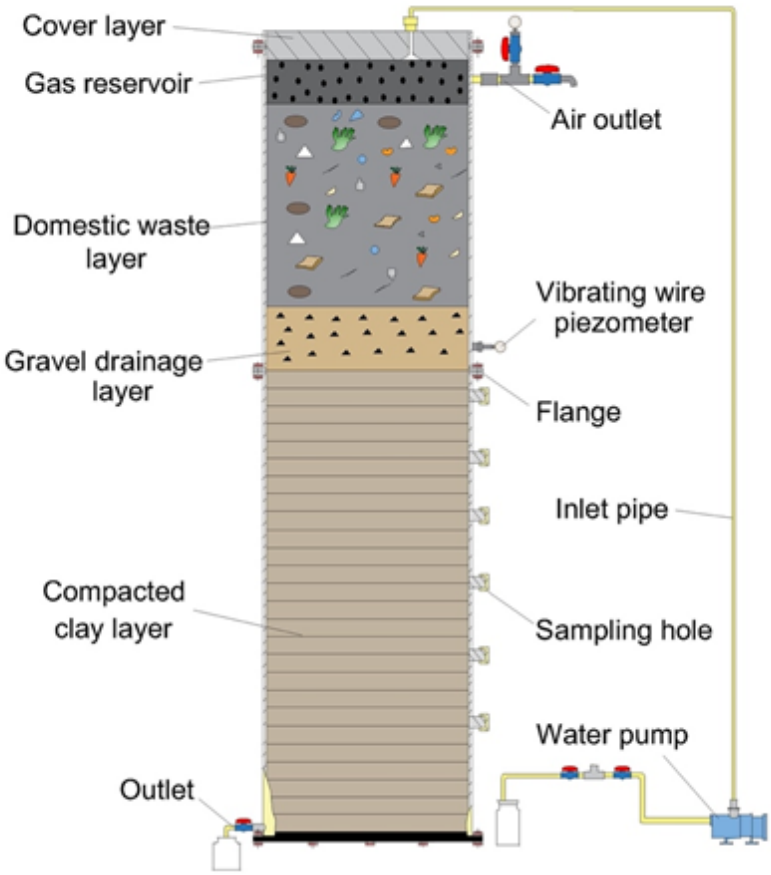

Figure 1

Schematic of experimental setup: municipal domestic waste,

gravel drainage and compacted clay layers

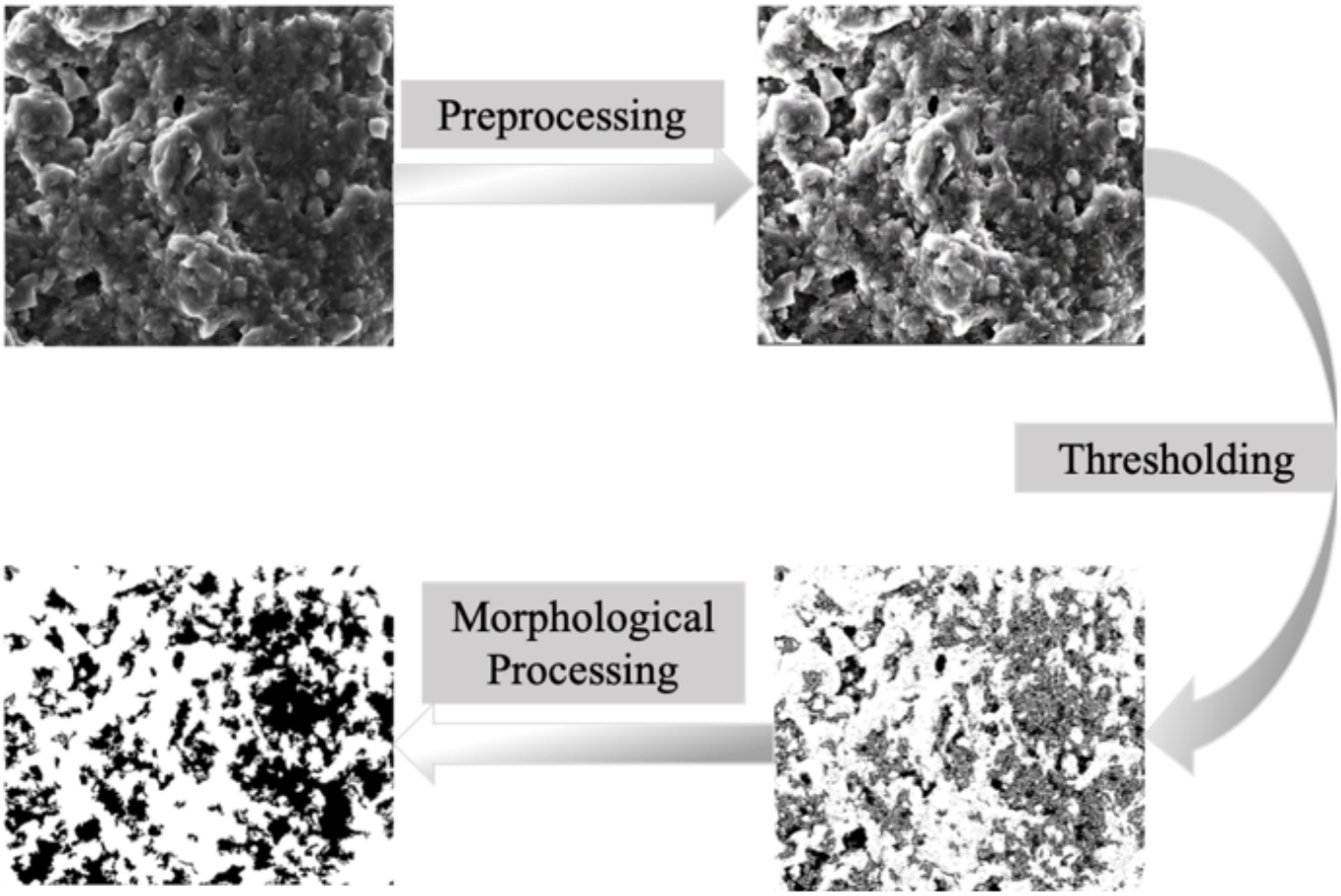

Figure 2

SEM images preprocessing of the uncontaminated clay sample

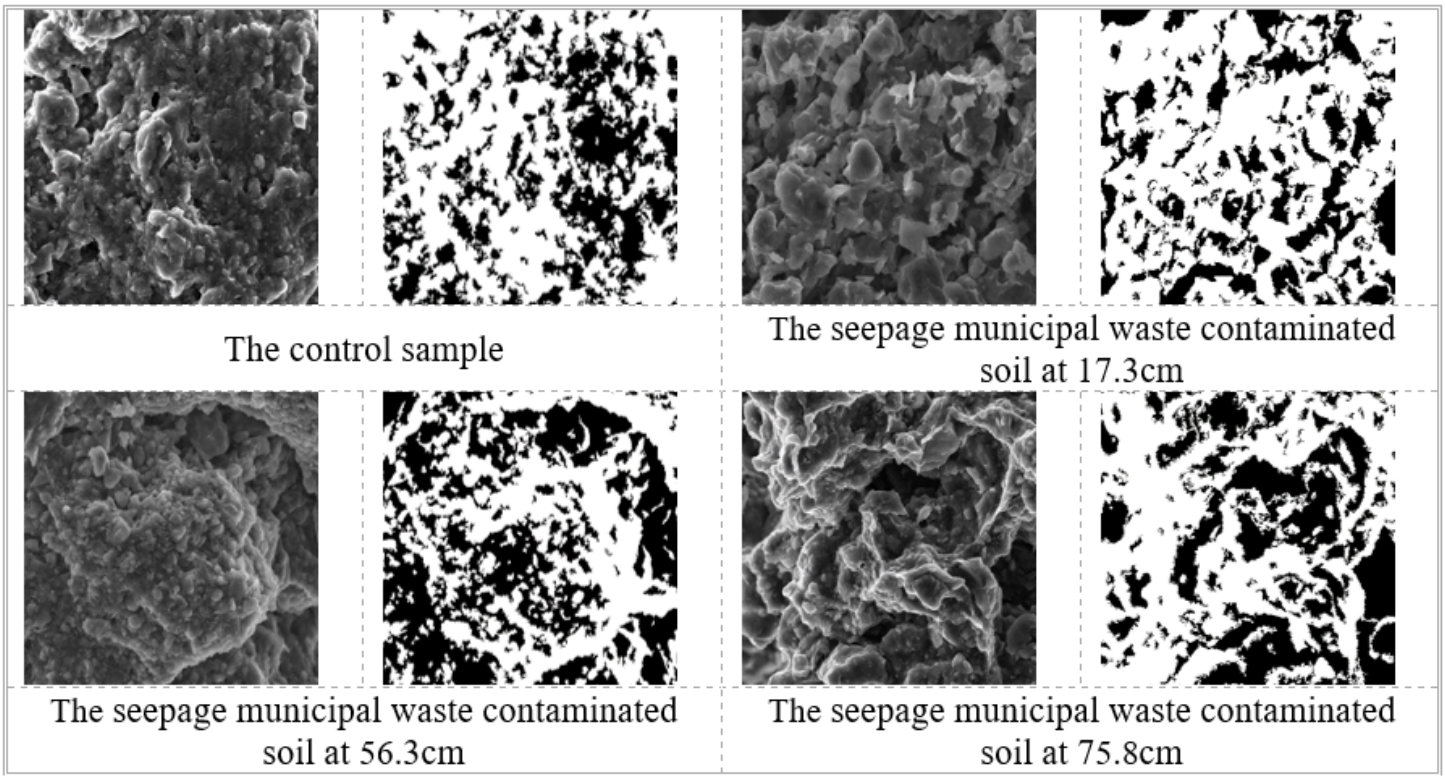

Figure 3

SEM images and binary images of control sample and contaminated clay with different seepage depths at 1500 magnification

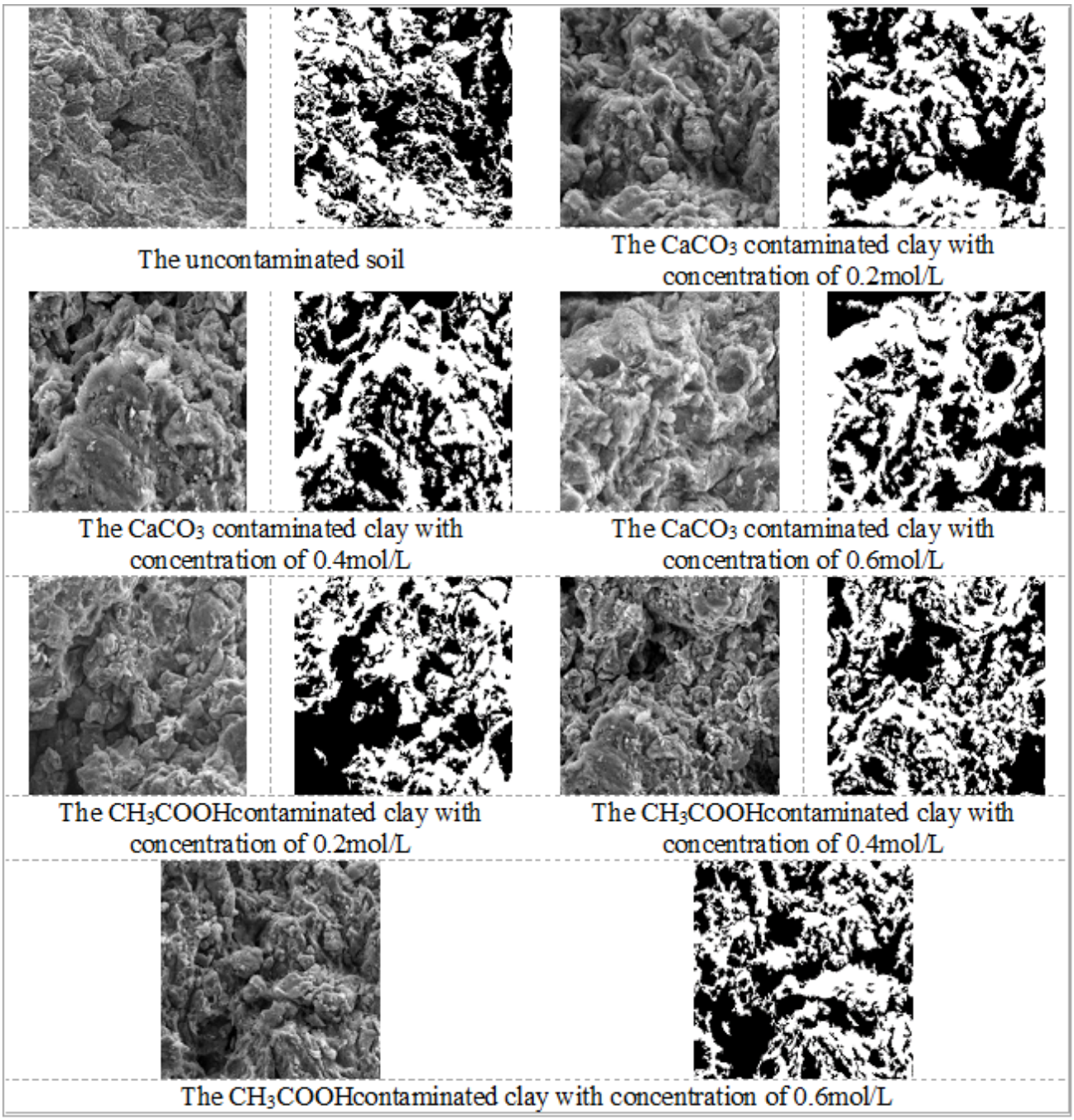

Figure 4

SEM images and binary images of uncontaminated soil and contaminated soil with different concentrations at 1200 magnification

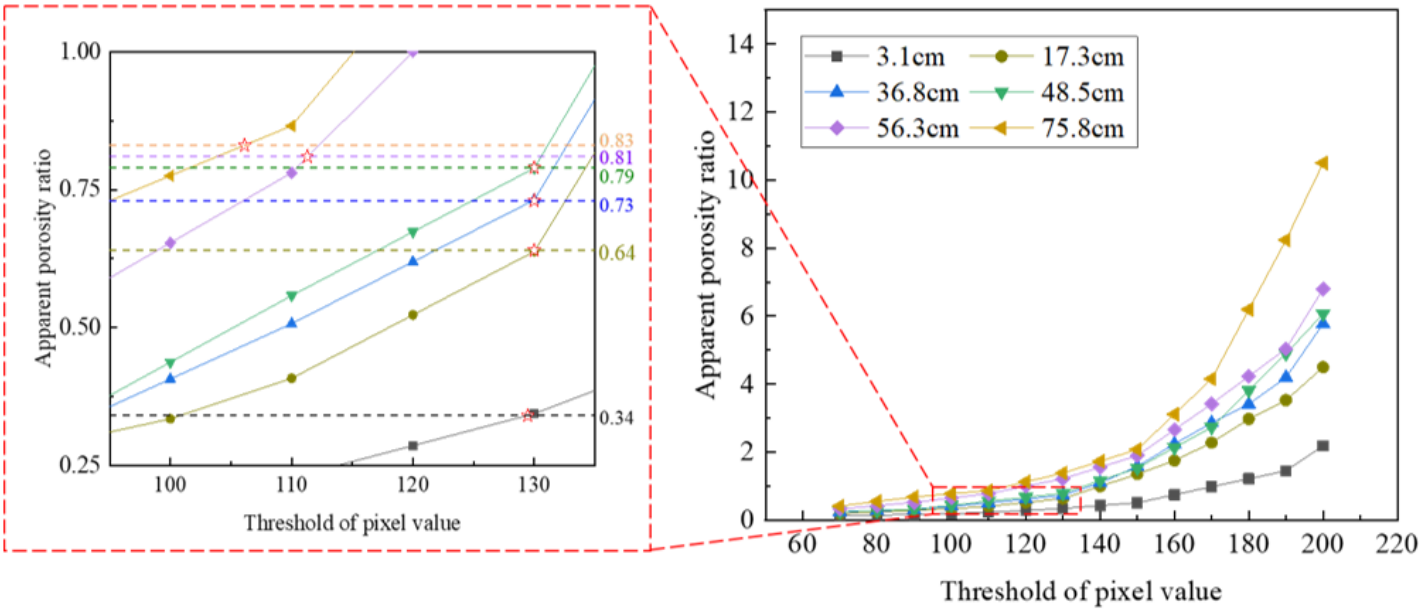

Figure 5

Relationship between apparent porosity ratio and pixel threshold values of samples at different column depths

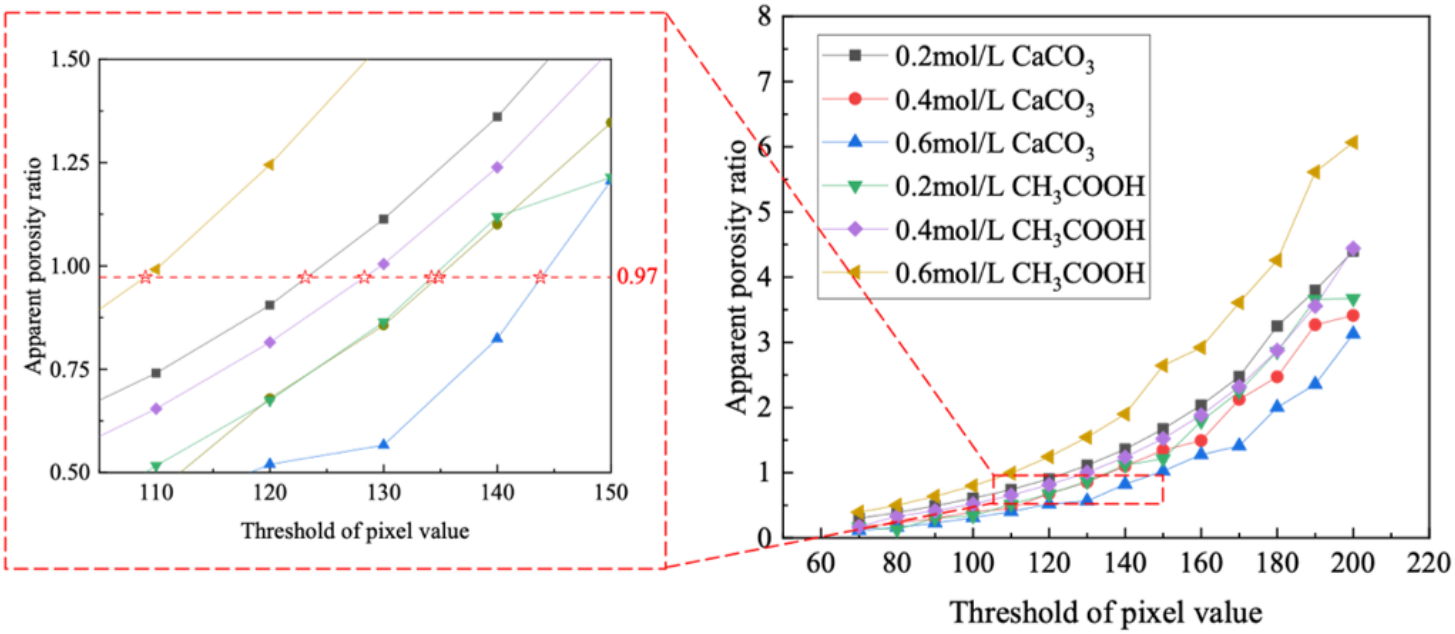

Figure 6

Relationship between apparent porosity ratio and pixel threshold values of samples at different concentrations

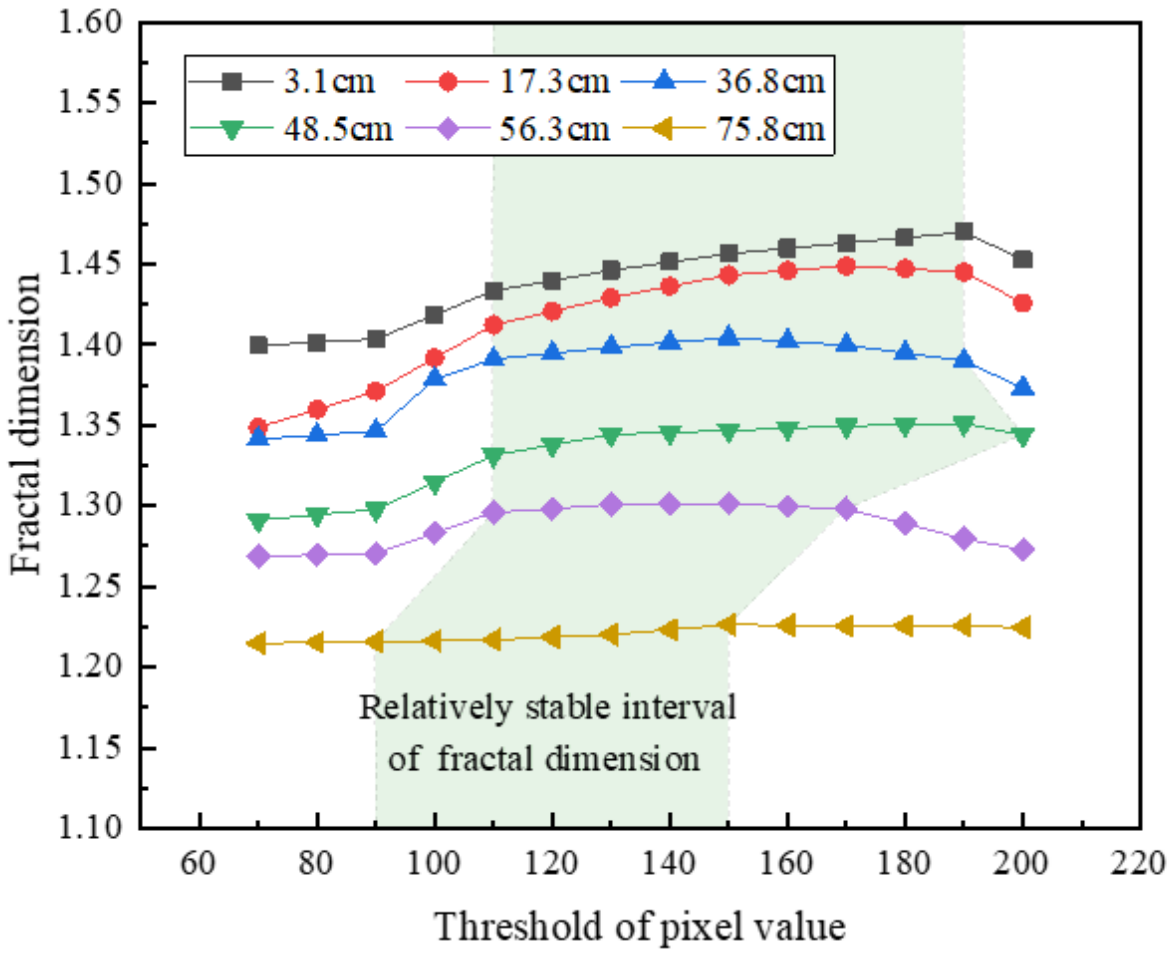

Figure 7

Relationship between fractal dimension and pixel value of clay particles at different column depths

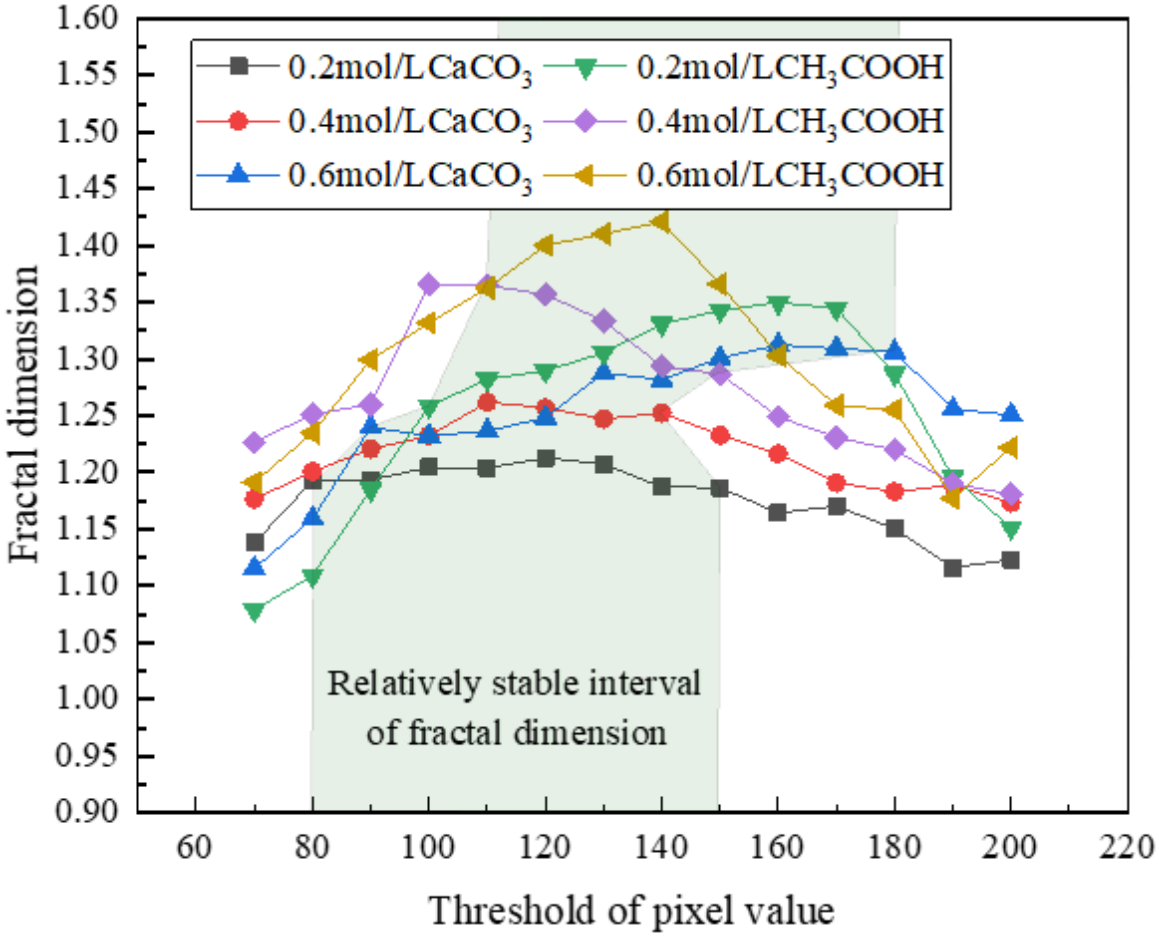

Figure 8

Relationship between fractal dimension and pixel value of clay particles at different concentrations

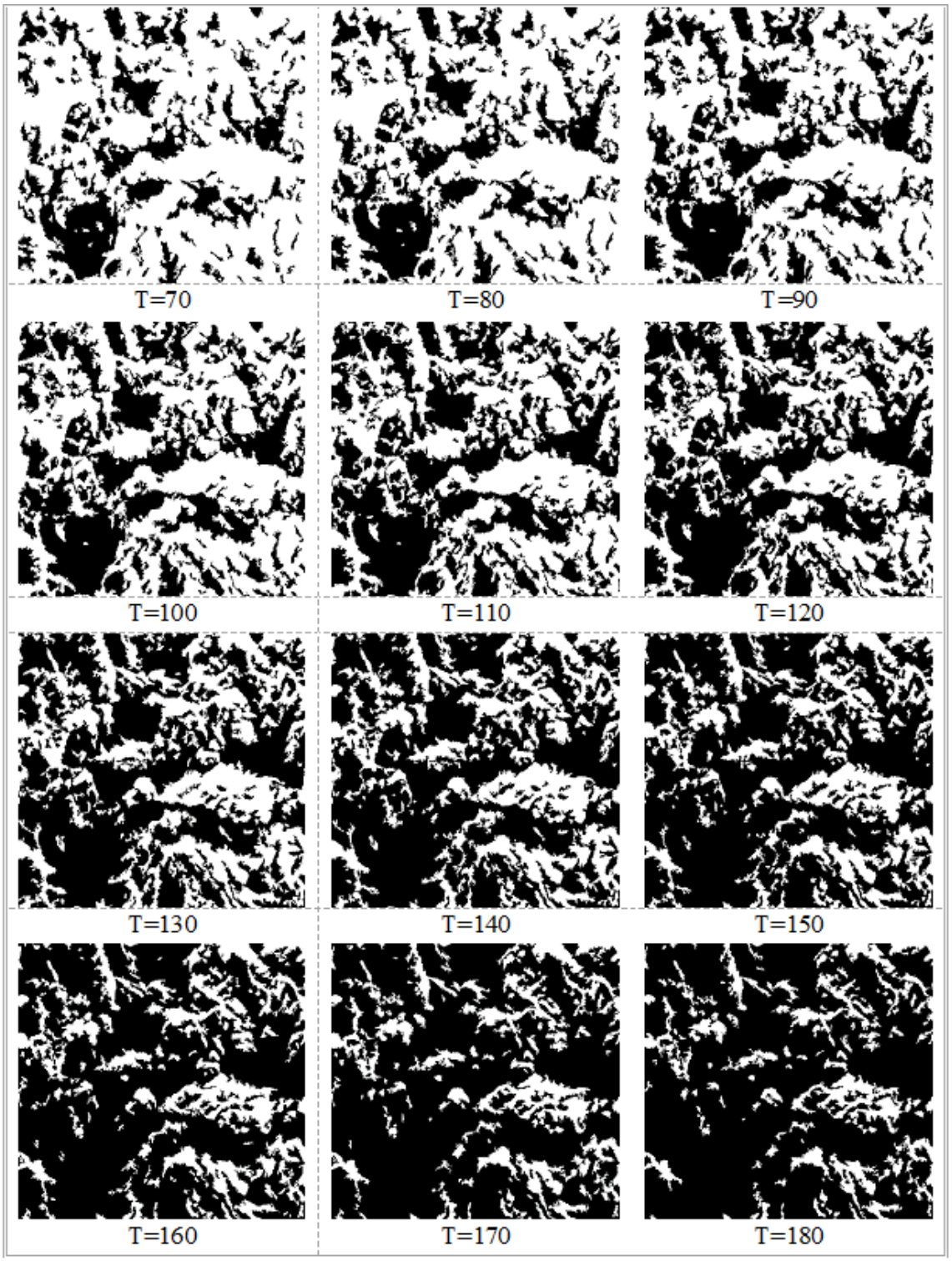

Figure 9

Binarization of SEM images of CH_3COOH contaminated clay with concentration of 0.6mol/L segmented by different pixel values

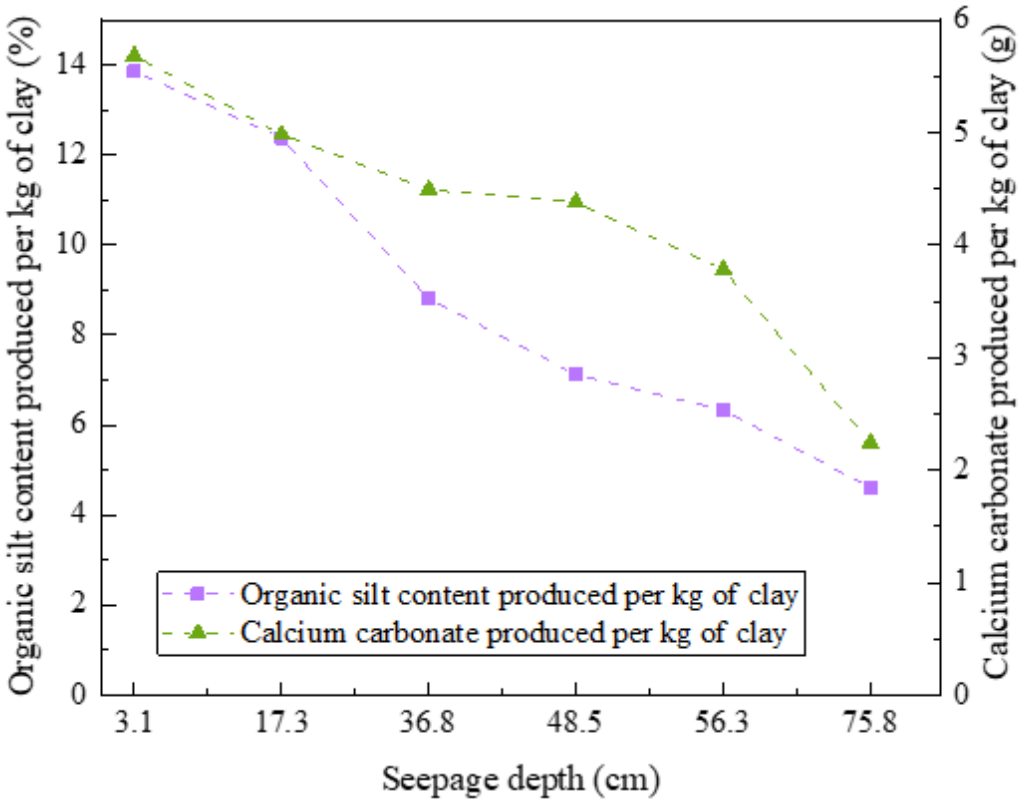

Figure 10

Amount of organic matter and calcium carbonated produced per kilogram of clay

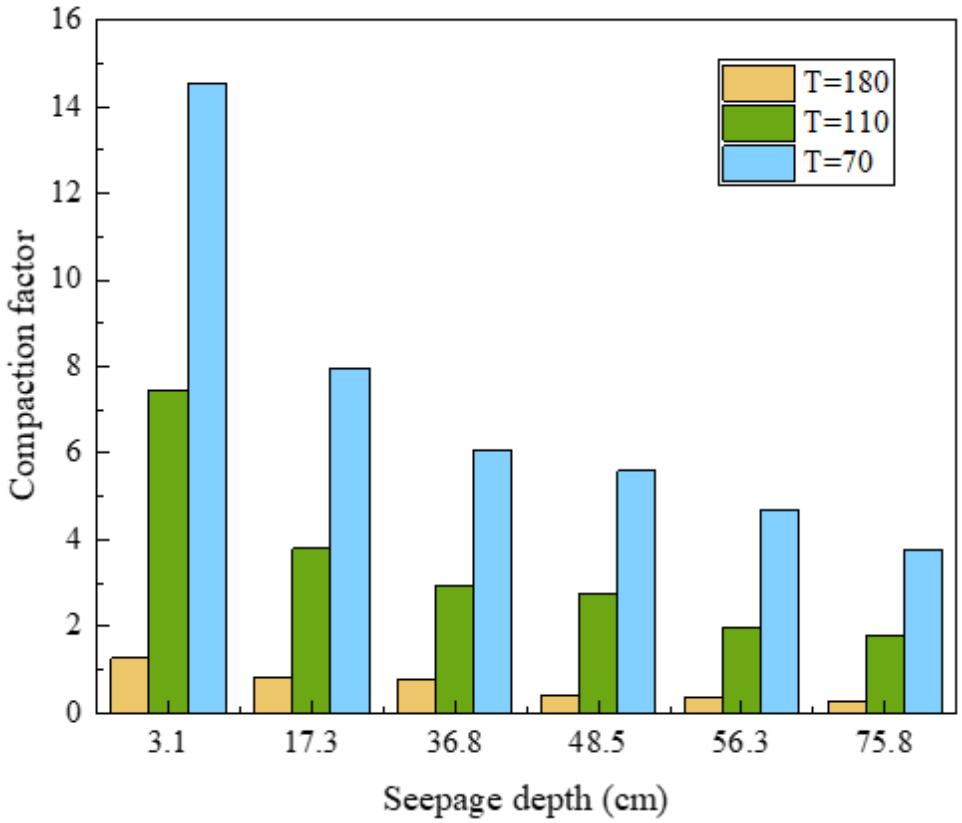

Figure 11

Relationship between compaction factor and seepage depth with different pixel threshold values

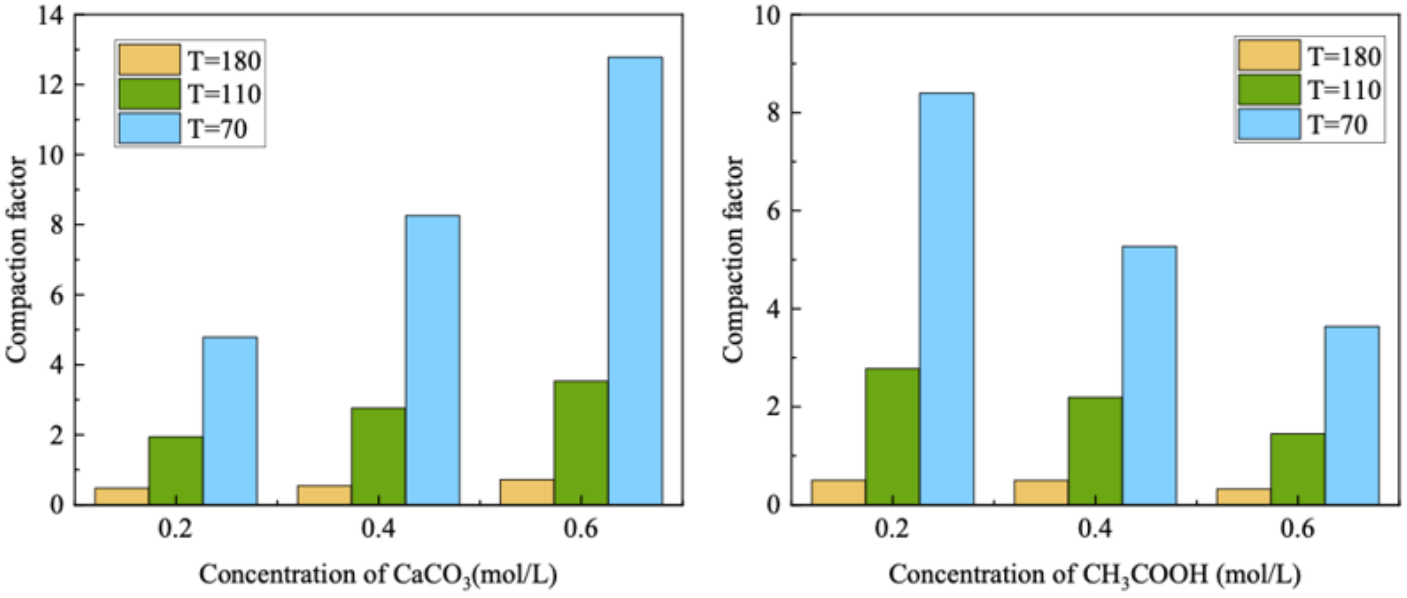

Figure 12

Relationship between compaction factor and concentration of contaminations with different pixel threshold values